SUPERSHELLS IN THE M 33 GALAXY

- A. Leščinskaitė^{1,2}, R. Stonkutė¹ and V. Vansevičius^{1,2}
- Center for Physical Sciences and Technology, Savanoriy 231, Vilnius LT-02300, Lithuania; alina.lescinskaite@ftmc.lt
- ² Vilnius University Observatory, Čiurlionio 29, Vilnius LT-03100, Lithuania; vladas.vansevicius@ff.vu.lt

Received: 2015 October 12; accepted: 2015 October 30

Abstract. We report preliminary results of the study of 18 supershells located in the Southern arm of the M 33 galaxy. Their age, size, and expansion velocity were determined and compared with the parameters of the H I holes detected in M 33. We conclude that the accurate identification of the supershells from H I observations can be effectively supplemented by simultaneous use of the H α , CO, and dust emission maps, as well as resolved stellar photometry data.

Key words: galaxies: individual (M 33) – galaxies: ISM: supershells

1. INTRODUCTION

Numerous observations of the Milky Way and other nearby gas-rich galaxies show that supershell structures, ranging in size from ~ 0.1 to ~ 1 kpc, are abundant in the interstellar medium (ISM) (Chu 2008). Giant cavities in the H I gas galaxy disk are created by combined effects of stellar feedback from multiple OB associations. The star formation produces aged stellar populations residing well inside the cavity and young OB associations along its periphery. Strong stellar winds and numerous supernovae (SNe) explosions result in continuous injection of energy into the surrounding ISM for up to $\sim 5 \cdot 10^7$ years, pushing out the surrounding gas. Energies required to clear out the interior of supershells are of the order of $10^{50}-10^{54}$ erg (McCray & Kafatos 1987).

As the supershell expands, it either disrupts the existing structures of the interstellar gas or accumulates the ambient matter, creating a layer of gas of increased density and an uneven distribution of clumpy gas clouds at the rims. The layer might become unstable and fragment, creating the environment suitable for secondary star formation to occur (Ehlerová & Palouš 2002). Interaction between two expanding supershells might increase the efficiency of molecular cloud formation at the rims of the shells and, consequently, create favorable conditions for induced star formation (Ntormousi et al. 2011).

As formation of the supershells in ISM appears to be a frequently occurring phenomenon, analysis of their properties and spatial distribution could provide us some clues on propagating star formation. For the present study we selected M 33, which is an apparently isolated dwarf spiral galaxy in the Local Group (Fig. 1a).

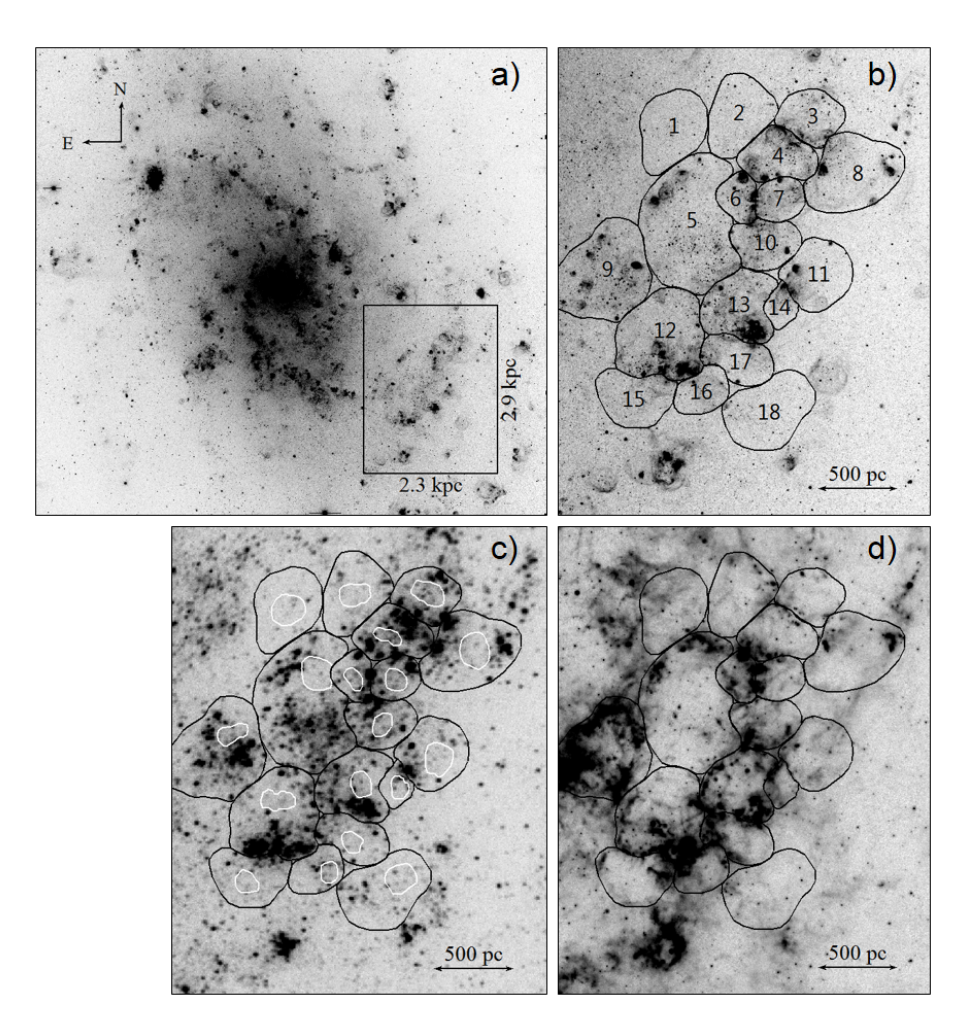


Fig. 1. Panels: a) $H\alpha$ -band image of the M 33 galaxy, the boxed area marks the field analyzed in this study; b) an enlarged image of the boxed area, the black contours mark the boundaries of identified supershells and numbers indicate their IDs; c) FUV emission map (GALEX), the white contours mark the boundaries of the oldest stellar population areas; d) dust emission (Spitzer/IRAC, $8\,\mu\mathrm{m}$). North is up, East is to the left.

The following parameters of M 33 are adopted in this study: 1) center coordinates of the galaxy: R.A. = $1^{\rm h}33^{\rm m}50.91^{\rm s}$, Dec. = $+30^{\circ}39'35.5''$ (J2000.0); 2) disk inclination angle $i=55^{\circ}$, and major axis position angle $P.A.=23^{\circ}$ (HyperLeda¹); 3) true distance modulus $(m-M)_0=24.65$ mag (850 kpc) (Stonkutė et al. 2008); 4) foreground interstellar extinction E(B-V)=0.06 mag (Schlegel et al. 1998); 5) metallicity of the M 33 disk Z=0.005, based on oxygen abundance, $12+\log({\rm O/H})=8.25$, derived from 13 H II regions (Rosolowsky & Simon 2008) located in the studied field, and assuming solar metallicity, Z=0.0134, and oxygen abundance, $12+\log({\rm O/H})=8.69$, as given in Asplund et al. (2009).

 $^{^{1}~~\}mathrm{http://leda.univ-lyon1.fr/}$

In Section 2 we provide details of the datasets used in this study. The derived parameters of the supershells, such as their sizes, ages and expansion velocities, are presented in Section 3, together with a brief discussion of the results.

2. DATA

To investigate properties of the star formation process on a large scale, we selected a field with dimensions of $570'' \times 717''$ ($\sim 2.3 \times 2.9 \,\mathrm{kpc}$), covering a star forming complex located in the Southern arm of the M 33 galaxy (Fig. 1). We analyze multi-wavelength observational data from ground-based and space telescopes.

The images obtained by the Galaxy Evolution Explorer (GALEX) space telescope (Thilker et al. 2005) were used to analyze the distribution of massive hot stars emitting strongly in the ultraviolet (Fig. 1c). The images of M 33 in the near-UV (NUV) and far-UV (FUV) with spatial resolutions of 5.3"and 4.3", corresponding to \sim 22 pc and \sim 18 pc, respectively, were retrieved from the Mikulski Archive for Space Telescopes (MAST)².

The optical images of M 33 at the U and H α photometric passbands were taken from the Local Group Galaxies Survey (LGGS) (Massey et al. 2006). Resolved deep BV stellar photometry data (\sim 48500 stars located in the studied area), derived from the Subaru Suprime-Cam observations (Narbutis et al. 2016, in preparation), were employed to perform a more detailed analysis of the stellar populations.

Spitzer Space Telescope data from IRAC (8 μ m) and MIPS (24 μ m) instruments were used to trace the emission from dust. The angular resolution is 2" (8 pc) and 6" (25 pc) for the observations at 8 and 24 μ m, respectively. The images were obtained from the NASA Extragalactic Database (NED). Observations and data reduction are described in Tabatabaei et al. (2007) and McQuinn et al. (2007).

Data of atomic and molecular hydrogen emission at radio wavelengths were taken from Gratier et al. (2010): the 21 cm emission maps, derived from VLA observations with resolution of $17''(\sim70\,\mathrm{pc})$, were used to trace the distribution of atomic gas; the integrated intensity maps of CO(2-1) emission, obtained at millimeter wavelengths with the 30 meter telescope, operated by the Institut de Radio Astronomie Millimétrique (IRAM), with a resolution of $12''(\sim50\,\mathrm{pc})$, were used to trace the distribution of molecular gas.

3. RESULTS AND DISCUSSION

3.1. Sizes of the supershells

Boundaries of the supershells were determined by visual inspection of multi-wavelength observational data. Based on the assumption that supershells are formed as a result of strong stellar feedback from the OB associations, the following features were taken into account: 1) holes in the disk of HI gas; 2) young star forming regions (OB associations, HII regions); 3) accumulations of molecular gas and dust (sites providing favorable conditions for secondary star formation) surrounding the HI holes. In the cases where a continuous distribution of the accumulated matter was not present at the rims of the shells (due to a strong disrupting effect from the initial OB associations), young stellar systems and/or

² http://galex.stsci.edu/GR6/?page=downloadlist&tilenum=5430

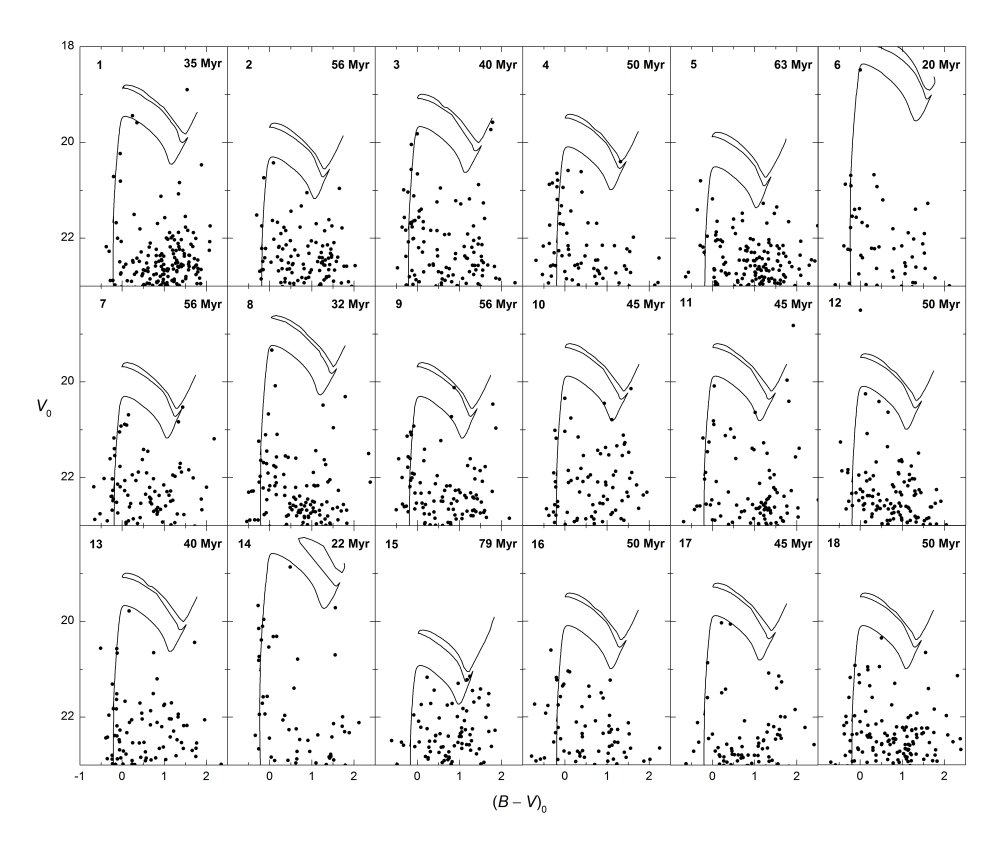


Fig. 2. The color-magnitude diagrams of the oldest stellar populations in the supershells (stars enclosed within the white contours in Fig. 1c), with PARSEC isochrones of Z=0.005 overlaid. Stellar photometry data (black dots) are from Narbutis et al. (2016, in preparation). Indicated in each panel are the supershell's ID number (Fig. 1b) and the estimated age (i.e., the age of the plotted isochrone). All isochrones are shifted by a distance modulus of 24.65 mag (Stonkutė et al. 2008). Stars are de-reddened according to the foreground MW extinction E(B-V)=0.06 mag (Schlegel et al. 1998).

individual accumulations of gas were used to trace the shapes of supershells. In total, 18 supershells were identified in the selected field (Fig. 1).

The effective diameter of a supershell was estimated as follows: $D_{\rm eff} = (D_{\rm max} + D_{\rm min})/2$, where $D_{\rm min} = 2\,(A_i/\pi)^{1/2}$ and $D_{\rm max} = P_i/\pi$. $A_i = A/\cos i$ is the area of a supershell, corrected for the galaxy inclination, $i = 55^{\circ}$, where A is a projected area of a supershell in square parsecs; $P_i = P/(2\cos i) + P/2$ is the perimeter of a supershell corrected for inclination, where P is a projected perimeter of a supershell in parsecs. An uncertainty of the diameter of a supershell is defined as $\sigma_D = (D_{\rm max} - D_{\rm min})/2$.

3.2. Ages of the supershells

After $\sim 50\,\mathrm{Myr}$ since its formation an OB association is no longer prominent, as the most massive stars have exploded and the weakly gravitationally bound system has spread out (McCray & Kafatos 1987). However, the initial stellar population is still detectable inside the supershell. We assume the age of stellar populations

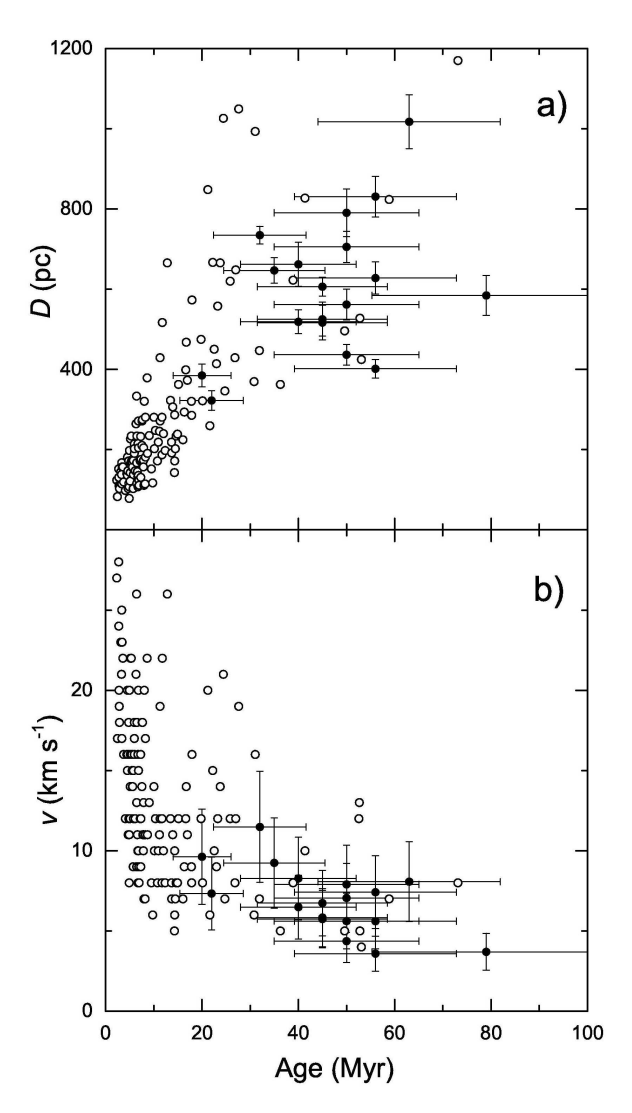


Fig. 3. Panels: a) the size vs. the age for the supershells identified in the studied field (filled circles) and for the HI holes (open circles) identified by Deul & den Hartog (1990) in the M33 galaxy; b) the velocity of the propagating star formation in the identified supershells (filled circles) and the expansion velocity of the HI holes (Deul & den Hartog 1990) (open circles) vs. the age of a given structure.

to be equal to 0 at the rims of the supershell, therefore, the age of the old stellar population within the supershell (Fig. 1c) indicates the age of the structure.

The regions of the lowest surface number density of massive young stars and relatively free of molecular and dust emission were selected in each supershell to estimate the age of its oldest stellar population (see the white contours in Fig. 1c). The color-magnitude diagrams for the selected regions (Narbutis et al. 2016, in preparation) with the superimposed theoretical PARSEC isochrones of Z=0.005

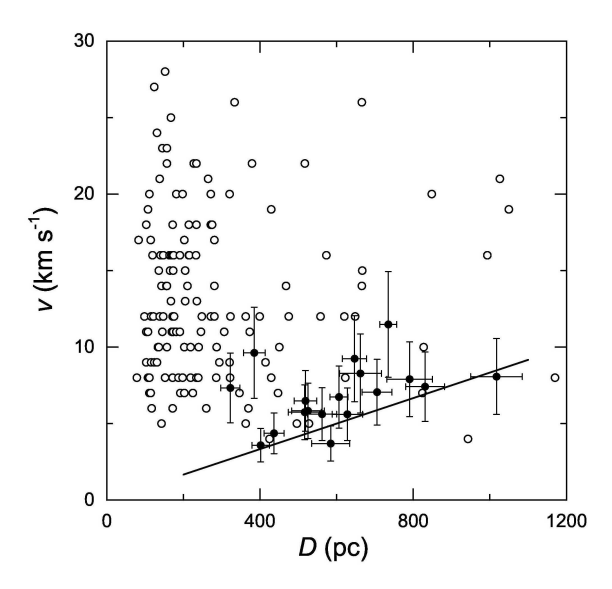


Fig. 4. The velocity of propagating star formation in the identified supershells (filled circles) and the expansion velocity of the HI holes (Deul & den Hartog 1990) (open circles) vs. the size of a given structure. The expansion velocities of the HI holes are accurate to 2 km s^{-1} , and their age errors are $\sim 30 \,\%$. Solid line indicates the selection limit for the supershell age $60 \,\text{Myr}$.

(release v1.2S, Bressan et al. 2012, Chen et al. 2014, Tang et al. 2014, Chen et al. 2015)³ were used to determine ages of the supershells (Fig. 2).

Rough estimates of errors in the derived supershell ages are of $\sim 30 \%$, in accordance with the age uncertainties of the HI holes declared by Deul & den Hartog (1990) whose data we use for comparison (Figs. 3 and 4).

3.3. Velocity of propagating star formation

Deul & den Hartog (1990) found HI holes in the M 33 galaxy to be well correlated with the OB associations, making their feedback a likely mechanism for causing formation of the HI holes and, possibly, the supershells analyzed in this study. The expansion velocities, estimated by Deul & den Hartog (1990), are accurate to 2 km s^{-1} , and their age errors are $\sim 30 \%$. The ages of the HI holes were derived from the diameter and expansion velocity: D/(2 v). We corrected the diameters of the HI holes for the difference in the adopted distance modulus for M 33.

We calculated the velocity of propagating star formation within the identified 18 supershells by making a simplified assumption that it was constant during the entire expansion time. Therefore, the expansion velocity of any supershell is equal to the ratio of its effective radius to age: $D/(2 \times \text{age})$.

The parameters of the supershells, identified in the Southern spiral arm of the M 33 galaxy (Fig. 1), were used to study properties of star formation on a large scale (Figs. 3 and 4). Note, however, that Deul & den Hartog (1990) identified only high contrast H I holes, thus their sample contains mainly compact struc-

 $^{^3}$ http://stev.oapd.inaf.it/cmd

tures, leaving out most of the larger and more evolved ones due to interfering inhomogeneous interstellar medium. On the other hand, the supershells analyzed in this study are strongly biased towards the larger objects due to the method applied for the age determination.

The two data sets, when compared, seem to follow the same overall trends in the parameter space (Fig. 3). The diameters of the supershells increase (Fig. 3a) and the expansion velocities decrease (Fig. 3b) as the structures age. This implies that supershells are expanding at decreasing rate as they evolve. An apparent increase in expansion velocity with increasing diameter of the supershell, seen in Fig. 4, is caused by selection effects, as illustrated by the solid line drawn for a fixed age of 60 Myr.

Analysis of supershells, using multi-wavelength observational data, provides us with information about late stages of their evolution as well as propagating star formation in general. We note that within supershells the secondary star formation is induced by making favorable conditions at their rims: accumulation and/or compression of surrounding gas increase the probability for star formation to take place. Also, we note that the derived parameters of supershells are in good agreement with the results, obtained by analyzing the HI holes in the M 33 gas disk, and extend them to the later supershell stages and larger sizes. Therefore, accurate identification of the supershells by using HI observations can be effectively supplemented by employing ${\rm H}\alpha$, CO, and dust emission maps, as well as resolved stellar photometry data.

ACKNOWLEDGMENTS. We are thankful to Donatas Narbutis for providing us with M 33 stellar photometry data prior to publication. This research was partly funded by a grant No. MIP-092/2015 from the Research Council of Lithuania.

REFERENCES

Asplund M., Grevesse N., Sauval A. J., Scott P. 2009, ARA&A, 47, 481

Chu Y.-H. 2008, in Massive Stars as Cosmic Engines (IAU Symp. 250), eds. F. Bresolin, P. A. Crowther & J. Puls, Cambridge University Press, Cambridge, p. 341

Bressan A., Marigo P., Girardi L. et al. 2012, MNRAS, 427, 127

Chen Y., Bressan A., Girardi L. et al. 2015, MNRAS, 452, 1068

Chen Y., Girardi L., Bressan A. et al. 2014, MNRAS, 444, 2525

Deul E. R., den Hartog R. H. 1990, A&A, 229, 362

Ehlerová S., Palouš J. 2002, MNRAS, 330, 1022

Gratier P., Braine J., Rodriguez-Fernandez N. J. et al. 2010, A&A, 522, A3

Massey P., Olsen K. A. G., Hodge P. W. et al. 2006, AJ, 131, 2478

McCray R., Kafatos M. 1987, ApJ, 317, 190

McQuinn K. B. W., Woodward C. E., Willner S. P. et al. 2007, ApJ, 664, 850

Ntormousi E., Burkert A., Fierlinger K., Heitsch F. 2011, ApJ, 731, 13

Rosolowsky E., Simon J. D. 2008, ApJ, 675, 1213

Schlegel D., Finkbeiner D., Davis M. 1998, ApJ, 500, 525

Stonkutė R., Vansevičius V., Arimoto N. et al. 2008, AJ, 135, 1482

Tabatabaei F. S., Beck R., Krause M. et al. 2007, A&A, 466, 509

Tang J., Bressan A., Rosenfield P. et al. 2014, MNRAS, 445, 4287

Thilker D. A., Bianchi L., Boissier S. et al. 2005, ApJ, 619, 67